# A laser spectroscopic study on $Xe^+$ ion transport phenomena in a 5 kW-class Hall effect thruster.

**IEPC-2007-160**

*Presented at the 30th International Electric Propulsion Conference, Florence, Italy*
*September 17-20, 2007*

S. Mazouffre*, D. Gawron†, V. Kulaev‡
*CARE Institute – CNRS, 1c Av. de la Recherche Scientifique, 45071 Orléans - France.*

*and*

N. Sadeghi§
*Laboratoire de Spectrométrie Physique, Université Joseph Fourier – CNRS,*
*140 Av. de la Physique, BP 87, 38402 Saint Martin d'Hères - France*

**Abstract: The Velocity Distribution Function (VDF) of metastable $Xe^+$ ions was measured along the channel axis of the 5 kW-class PPS®X000 Hall thruster by means of Laser Induced Fluorescence spectroscopy at 834.72 nm for various voltages, magnetic fields and mass flow rates. Axial velocity and dispersion profiles are compared to on-axis profiles obtained with the 1.5 kW-class PPS100 thruster. Outcomes of the comparison are threefold. (i) The broadening of the FDV across the region of strong magnetic field is a general feature for Hall thruster. It originates in the overlap between ionization and acceleration layers. The velocity dispersion increases with the discharge voltage; it reaches up to 200 eV in unit of kinetic energy at 700 V. (ii) Most of the acceleration potential (~70 %) is localized outside the thruster channel whatever the thruster size and operating conditions. The electric field moves upstream when the applied voltage is ramped up; in other words the fraction of potential inside the channel increases with the voltage; (iii) A non negligible amount of very slow and very fast (kinetic energy higher than the applied potential) $Xe^+$ ions are always observed. Such ions may find their origin in space and temporal oscillations of the electric field as suggested by numerical simulations carried out with a hybrid model.**

**For the first time ever the temporal characteristics of the $Xe^+$ ion VDF was recorded in the course of low-frequency discharge current oscillations with a time resolution of 100 ns. As the number of fluorescence photons is very low during such a short time period, we developed a pulse-counting lock-in system able to perform real-time discrimination between background and LIF photons. The evolution in time of the VDF was observed at several locations along the channel axis after fast shut down of the thruster power. The anode discharge current is switched off at 2 kHz during 5 μs without synchronization with the current oscillation cycle. Measurements clearly show that the axial component of the $Xe^+$ ion velocity does vary in time, which means the electric field changes in time. Time-resolved LIF experiments therefore bring to light new insights into the physics of a HET.**

* Research Scientist at CNRS, EP team of the CARE institute, stephane.mazouffre@cnrs-orleans.fr.
† PhD student, EP team of the CARE institute, gawron@cnrs-orleans.fr.
‡ Graduated student, EP team of the CARE institute, kulaev@cnrs-orleans.fr.
§ Research Scientist at CNRS, University of Grenoble, nader.sadeghi@ujf-grenoble.fr.

## Nomenclature

| | | |
|---|---|---|
| **B** | = | magnetic field (Gauss) |
| $\Delta$Ec | = | dispersion in kinetic energy (eV) |
| **E** | = | electric field (V/cm) |
| Ec | = | kinetic energy (eV) |
| $\Phi_a$ | = | xenon anode mass flow rate (mg/s) |
| $I_c$ | = | solenoid current (A) |
| $I_d$ | = | discharge current (A) |
| **k** | = | laser beam wave vector |
| $\lambda$ | = | wavelength (nm) |
| $\nu$ | = | light frequency (Hz) |
| p | = | velocity dispersion (m/s): $p = 2.355\times\sigma$ |
| $\sigma$ | = | velocity dispersion or standard deviation (m/s) |
| t | = | time (s) |
| $U_{acc}$ | = | acceleration potential (V) |
| $U_d$ | = | discharge voltage (V) |
| v | = | $Xe^+$ ion velocity in the x direction (m/s) |
| $v_{max}$ | = | maximum ion velocity (m/s) |

## I. Introduction

EXAMINATION of ion transport phenomena in the low-pressure E×B discharge of a Hall Effect Thruster (HET) is one way to improve our understanding about the physical processes at work in this specific type of plasma source used for propulsion of satellites and interplanetary probes. As $Xe^+$ ions are not magnetized in a HET, the ionic flow is solely driven by the electric field. By measuring the ion velocity it is possible to reconstruct the accelerating potential and therefore the electric field, the latter being directly linked to the anomalous electron diffusion across the magnetic barrier. Moreover, the spread in the ion kinetic energy is a direct consequence of the degree of interaction between the ionization and acceleration layers. The highest value of the kinetic energy ions can reach under a given set of Hall thruster operating parameters, which is usually above the applied potential, is also a relevant data as it furnishes with valuable information about the electric field dynamics.

Laser Induced Fluorescence (LIF) spectroscopy has been often used in the past few years to measure the velocity of metastable ions in the plasma of a HET[1,2,3,4]. In this contribution we present spatially-resolved as well as time-resolved measurements of the $Xe^+$ ion Velocity Distribution Function (VDF) in the discharge chamber and in the plasma plume of the 5 kW-class PPS®X000 Hall effect thruster[5] performed by means of Laser Induced Fluorescence spectroscopy in the near infrared. Ion VDFs were measured parallel to the thruster axis, i.e. in the ion flow direction, for a broad range of discharge voltage (300 V – 700 V) and magnetic field strength (12 A – 20 A current in the coil) at constant gas flow rate (6 mg/s). A high flow rate condition (9 mg/s) was also investigated. The evolution in time of the VDF was measured for one operating conditions (500 V, 6 mg/s) at various locations during the transient regime that follows a fast anode discharge current ignition in order to investigate the ion dynamics during forced and free low frequency current oscillations. The current is switched off during 5 µs at a 2 kHz repetition rate without any synchronization with the discharge current oscillation cycle. On-axis profiles of the time-averaged ion axial velocity, kinetic energy dispersion profiles and electric field distributions are presented and compared with the ones obtained with a 1.5 kW-class PPS100 thruster in order to investigate the effect of the size and the operating conditions. Contour plots of the time-varying $Xe^+$ ion VDF are shown for three positions along the channel axis. A possible explanation of the observed VDF behavior in terms of electric field oscillation is discussed in the final section of this article before giving concluding remarks.

## II. Experimental arrangement

### A. Metastable $Xe^+$ ion detection scheme

LIF spectroscopy is a non intrusive diagnostic tool that enables to determine the velocity of probed particles along the laser beam direction by measuring the Doppler shift of absorbed photons. As shown in Fig. 1, the transition used in the measurements presented in this paper is the $5d\ ^2F_{7/2} \rightarrow 6p\ ^2D^o_{5/2}$ at $\lambda_{air}$ = 834.723 nm, which

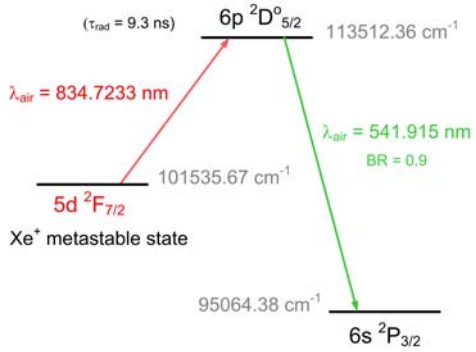


**Figure 1: Energy diagram of the LIF spectroscopy excitation and detection scheme for the measurement of metastable $Xe^+$ ion velocity distribution function in a HET.**

has been chosen due to a large population in the $5d\ ^2F_{7/2}$ metastable state of $Xe^+$ ion and due to the favorable branching ratio of the $\lambda_{air} = 541.915$ nm line originating from its upper state that allows non resonant LIF. Measuring the frequency ν at which the laser beam energy is absorbed allows to determine the ion Doppler shift. Therefore it is possible to calculate the ion velocity component corresponding to the laser beam direction by using the following equations:

$$\Delta\nu = \nu - \nu_0 = \frac{1}{2\pi}\mathbf{k}\cdot\mathbf{v}\,, \tag{1}$$

where Δν is the Doppler shift, **k** is the laser beam wave vector and **v** is the ion velocity vector. Under our conditions, vectors **k** and **v** are parallel. Equation 1 then reads:

$$v_x = c\frac{\nu - \nu_0}{\nu} \approx c\frac{\nu - \nu_0}{\nu_0}\,, \tag{2}$$

where c is the speed of light in a vacuum. In Eq. 1 and 2, $\nu_0$ is the studied transition unshifted frequency, and ν is the laser frequency. We have made our own precise measurement of the absolute value of $\lambda_0$ in a low-pressure stationary xenon RF discharge: $\lambda_0 = (834.7233 \pm 0.0001)$ nm in air.

It exits 9 stable isotopes of xenon, two of them having a nonzero nuclear spin. As a consequence the studied transition is made of 19 components. Most intense components form a distribution of which the full width at half maximum is around 600 MHz at 300 K. The hyperfine and isotopic structure, the mass effect and the Zeeman splitting are not accounted for in this work as the width of a measured FDV is typically above 3 GHz in the region of strong magnetic field due to physical processes at work in a HET, as we will see.

### B. Optical bench and Detection branch

The optical bench was extensively described in Ref. 3. The laser beam used to excite $Xe^+$ metastable ions is produced by an amplified tunable single-mode external cavity laser diode (MOPA TA100 from Toptica) that can deliver up to 700 mW of power in the near IR spectral domain. The laser remains mode-hop free over a frequency tuning range of more than 10 GHz. The spectral width of the laser beam profile is about 1 MHz. Behind the tapered amplifier the laser beam passes through a Faraday isolator to prevent optical feedback into the laser cavity. The wavelength is accurately measured by means of a calibrated WS/8UV wavemeter from HighFinesse whose absolute accuracy is better than 100 MHz, which corresponds to ~90 m/s. A plane scanning Fabry-Pérot interferometer with a 1.29 GHz free spectral range is used to real-time check the quality of the laser mode. The power of the beam is also continuously monitored. The primary laser beam is modulated by a mechanical chopper before being coupled into a 60 m long multi-mode optical fiber of 50 μm core diameter. The fiber allows to carry the beam into the vacuum chamber of the PIVOINE-2g ground-test facility. The fiber output is located behind the thruster. Collimation optics are used to form a narrow beam that passes through a 1.5 mm in diameter hole located at the back of the thruster.

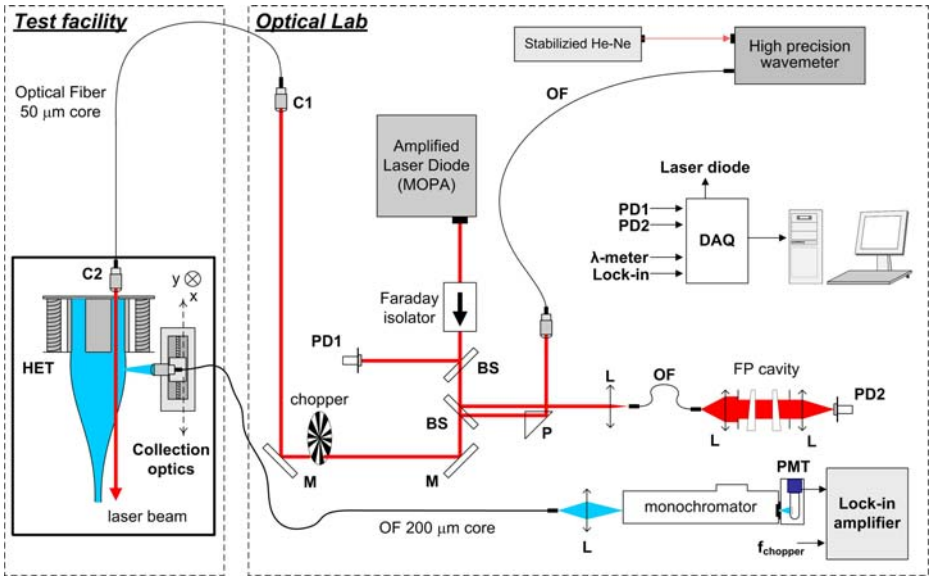


**Figure 2: Drawing of the LIF spectroscopy setup used to measured the time-averaged $Xe^+$ ion VDF in the plasma of the PPS®X000 Hall effect thruster.**
**OF: optical fiber; L: lens; M: mirror; P: prism; BS: beam splitter; PD: photodiode; C: collimator**

The laser beam propagates parallel to the channel axis in the direction of the ion flow. About 3 mW of light power are deposited into the detection volume. A schematic drawing of the complete optical bench is shown in Fig. 2.

A detection branch made of a 25.4 mm focal length, which focuses the fluorescence light onto a 200 µm core diameter optical fiber, is mounted onto a travel stage perpendicular to the channel axis as shown in Fig. 3. The magnification ratio is 1 meaning that the spatial resolution is 200 µm in axial direction. A 16 mm in length slit was made in the channel dielectric outer wall in order to carry out measurements inside the channel. The collection system allows to probe an area stretching from 16 mm into the channel up to 50 mm outside. The light is transported by way of the 200 µm fiber to a 20 cm focal length monochromator that isolates the 541.9 nm line from the rest of the spectrum. A Hamamatsu R928 photomultiplier tube serves as a light detector. A lock-in amplifier operating at the chopper frequency (200-400 Hz) is used to discriminate the fluorescence light from the intrinsic plasma emission. Scanning of the MOPA cavity, data acquisition (16 bits, 333 ks/s, PCI-6052E ADC from NI) and laser wavelength monitoring is computer controlled.

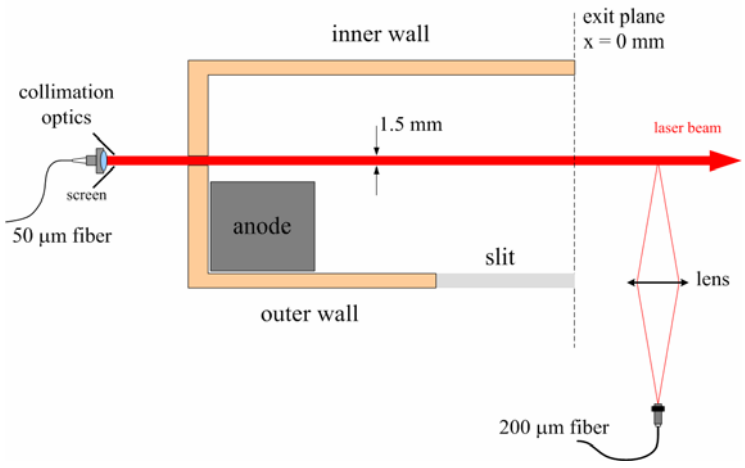


**Figure 3: Simplified drawing of the laser injection into the channel of the PPS®X000 thruster and of the detection branch.**

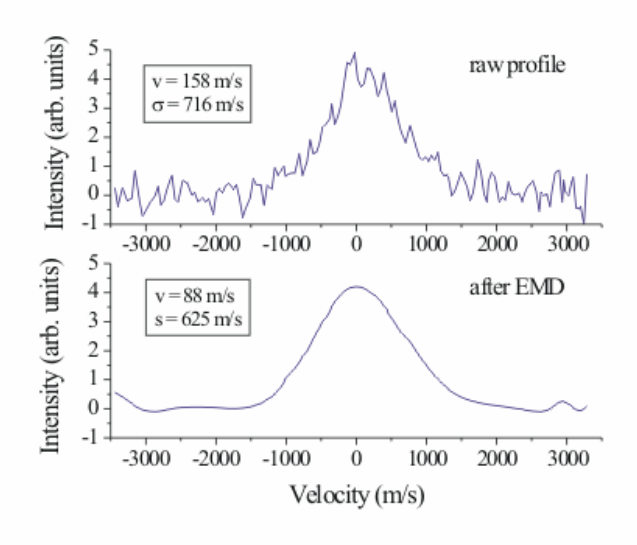


**Figure 4: Example of a VDF of $Xe^+$ metastable ions obatined by LIF. Top: raw distribution at 500 V, 15 A and 6 mg/s. Bottom: Distribution after smoothing by way of the EMD method (3 modes have been removed).**

## III. Analysis of recorded FDV – Quantities to be studied

### A. Smoothing procedure with EMD

Instead of classical smoothing technique like averaging we used the Empirical Mode Decomposition (EMD) method to reduce the noise level of the measured fluorescence spectra[6]. In short, the EMD is a self adaptative decomposition method that allows to split up any data series into its individual characteristic oscillations, so-called intrinsic mode functions, each mode having its own frequency scale and energy content. When applying EMD to an ion VDF measured by LIF, one typically obtains 6 to 7 modes and a residual. Data smoothing is then realized by removing the high frequency modes. In fact the smoothed signal corresponds to the sum of low frequency modes plus the residual. In our case, the advantage of this method is that it permits to easily separate electronic and plasma induced noise (HF part of the signal) from the fluorescence signal (LF part of the signal). However, the problem of the origin of mid-frequency part of the signal remains meaning that data treatment must anyway be done with care.

For most results presented in this contribution, the first three modes with highest frequencies have been removed. An example of data smoothing outcome based on the EMD is shown in Fig. 3. Of course the smoothing procedure must note modify the shape of the VDF. When suppressing 3 high frequency modes, the gap between the width, i.e. the standard deviation, of smoothed and raw profiles is always below ± 10 %, being most of the time below ± 5 %. As the noise level greatly influences the value of the standard deviation, the noticed gap is perfectly acceptable.

We are still working on a proper method for calculating error bars for the mean velocity and the standard deviation. One way is to use the upper and lower envelopes of the raw distribution. Another way is to use the EMD technique to break up the measured profile into two components, the "true" distribution and the noise; error bar would then be assessed from the noise standard deviation. So far, a statistical analysis of our dataset indicates that the error bar for the velocity dispersion is around ± 20 %.

### B. Quantities derived from the time-averaged $Xe^+$ ion VDF

Instead of comparing time-averaged ion VDF to one another, it is much wiser to analyze statistical quantities inferred from the moments of the VDF. The quantities studied in the next sections of this article are the following:

- the mean ion velocity v obtained from the first order moment of the velocity distribution,
- the velocity spread or dispersion σ that correspond to the standard deviation; it is computed from the second order moment of the distribution.

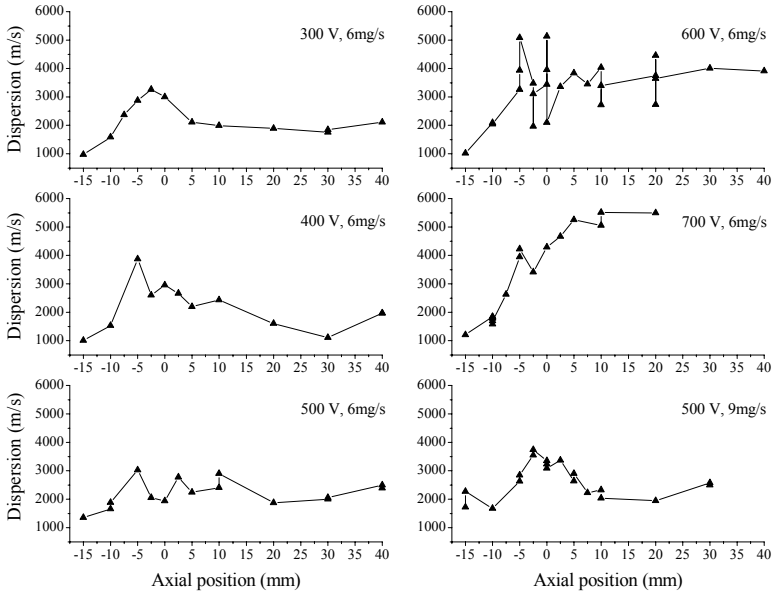


**Figure 5: Development of the $Xe^+$ ion axial velocity dispersion (p parameter) along the channel axis of the PPS®X000 thruster for various values of $U_d$ and $\Phi_a$. The channel exit is at x = 0 mm.**

Three other quantities are used:

- the so-called maximum ion velocity $v_{max}$; it corresponds to the velocity for which the amplitude of the distribution drops down to 10 % of its maximum value on the high velocity side[3,4]. The arbitrary 10 % factor is chosen to warrant an unambiguous definition of $v_{max}$ as the poor S/N ratio enables to accurately determine the true maximum velocity from the measured VDFs. In like manner, one can define a minimum velocity, considering the low velocity wing of the distribution.
- The p parameter which is another way to define the velocity dispersion. It reads:

$$p = 2\sqrt{2\ln(2)} \times \sigma \approx 2.335 \times \sigma. \tag{3}$$

  The quantity p is equal to the FWHM in the case of a Gaussian distribution. In the remainder of the paper the p parameter is used as a value of the dispersion.

- It is also interesting to calculate the spread in kinetic energy ΔEc to compare it with the applied potential energy $e\,U_d$, where $e$ is the elementary charge. In this work, the spread in kinetic energy is given by:

$$\Delta E_c = \frac{m}{e} \times v \times dv = \frac{m}{e} \times v \times p\,, \tag{4}$$

- where $m$ is the $Xe^+$ ion mass and v the mean velocity. ΔEc depends upon the velocity, therefore it increases when the fluid accelerates even if σ stays unchanged.

The most probable velocity is not used here. However, it value is closed to the mean velocity.

### C. PPS®X000 operating conditions

All measurements have been carried out in the PIVOINE-2g ground-test facility. The PPS®X000 thruster was equipped with BN-$SiO_2$ dielectric walls and a carbon anode.

During the experiments campaign, the applied voltage, the magnetic field strength as well as the mass flow rate have been changed is such a way that 9 distinct operating conditions have been used. The xenon gas flow rate

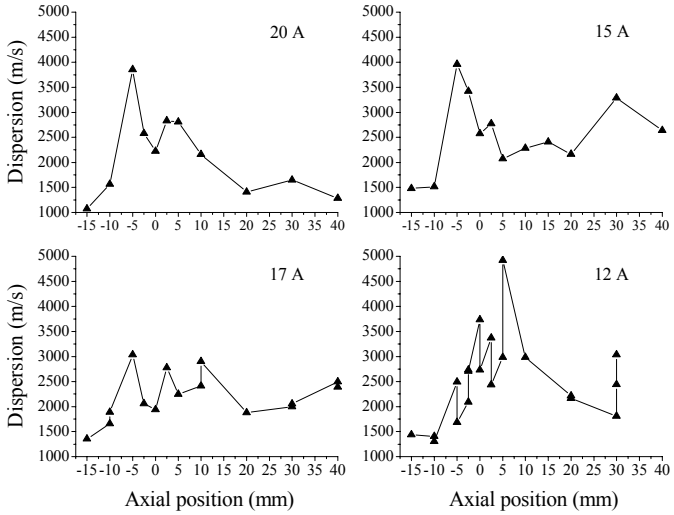


**Figure 6: Development of the $Xe^+$ ion axial velocity dispersion (p parameter) along the channel axis of the PPS®X000 thruster for various values of $I_b$ (change of the magnetic field).**

through the cathode was always kept fixed at 0.6 mg/s. The power range stretched from 1500 W to 4200 W. The background pressure inside the vacuum chamber was $1.4\times10^{-5}$ mbar-Xe for all conditions.

Operating conditions for the PPS®X000 thruster are summarized below:

- voltage series ($\Phi_a$ = 6 mg/s, $I_b$ = 17 A): $U_d$ = 300 V, 400 V, 500 V, 600 V, 700 V.
- magnetic field series ($U_d$ = 500 V, $\Phi_a$ = 6 mg/s): $I_b$ = 20 A, 17 A, 15 A, 12 A.
- mass flow rate series ($U_d$ = 500 V, $I_b$ = 17 A): $\Phi_a$ = 6 mg/s, 9 mg/s.

For information, during the measurement campaign of the $Xe^+$ ion VDF conducted with the PPS100 thruster, 7 distinct operating conditions were investigated. The operating parameters were[3,4]:

- voltage series ($\Phi_a$ = 5 mg/s, $I_b$ = 4.5 A): $U_d$ = 100 V, 200 V, 300 V.
- magnetic field series ($U_d$ = 200 V, $\Phi_a$ = 5 mg/s): $I_b$ = 5.5 A, 4.5 A, 3.5 A, 2.5 A.
- specific point with a low oscillation level: $U_d$ = 275 V, $I_b$ = 3.8 A, $\Phi_a$ = 3 mg/s.

## IV. Time-averaged $Xe^+$ ion VDF properties

### A. Velocity dispersion and spread in kinetic energy

As can be seen in Fig. 5 and 6, the $Xe^+$ ion VDF broadens along the x direction whatever the values of $U_d$, B and $\Phi_a$. Below 600 V, the dispersion in axial velocity goes through a maximum. The maximum value of p, which is around 3000-3500 m/s is reached in the vicinity of the exit plane of the channel. At and above 600 V, the dispersion seems to reach a plateau. In fact the maximum could be shifted downstream. The mass flow rate and the magnetic field do not influence much the velocity dispersion. On the contrary, the applied voltage has a drastic impact upon the value and the profile of the dispersion. First, the dispersion increases with $U_d$; it reaches ~5500 m/s at 700 V. The impact of $U_d$ is even more obvious when considering the spread in kinetic energy. On-axis profiles of $\Delta$Ec are shown in Fig. 7 and 8. Whereas $\Delta$Ec is around 70 eV at 500 V for all B field configurations, it reaches 200 eV at 700 V, i.e. 28 % of the applied potential energy. Second, the shape of the profile of p and $\Delta$Ec along the channel axis depend upon the voltage, as previously explained. The change in behavior (from a peak to a plateau) may be connected with the drop in thrust efficiency at high voltage reported for all high-power Hall effect thruster. The observed trend may be a sign for a sudden change in the physics at work. This change would occur when the discharge voltage $U_d$ is above a certain threshold.

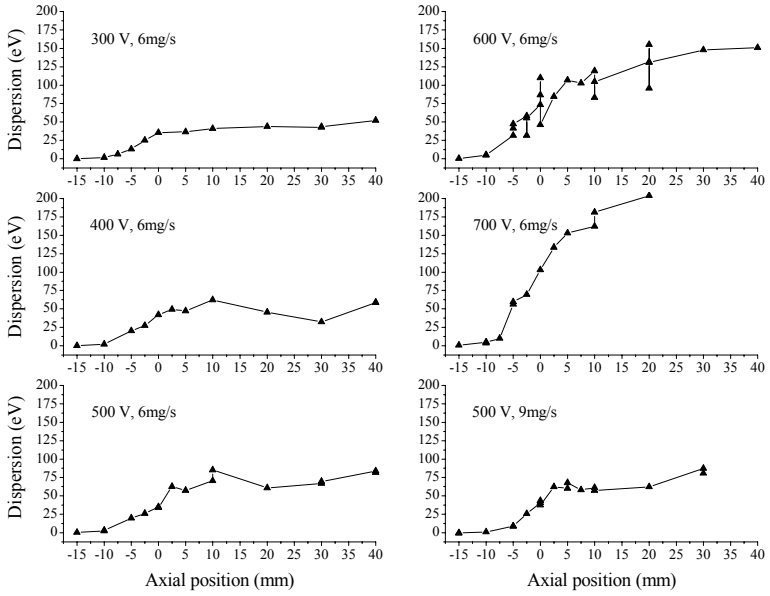


**Figure 7: Development of the spread in $Xe^+$ ion kinetic energy along the channel axis of the PPS®X000 thruster for various values of $U_d$ and $\Phi_a$.**

A large value of the $Xe^+$ axial velocity dispersion was also observed with a PPS100 thruster. The maximum value of p was of about 4000 m/s. The behavior with $U_d$ is identical.

The broadening of the $Xe^+$ ion VDF in the course of the flow and the large value of the velocity dispersion and of the spread in kinetic energy are at present well understood. They originate in the overlap between the ionization and the acceleration layers.

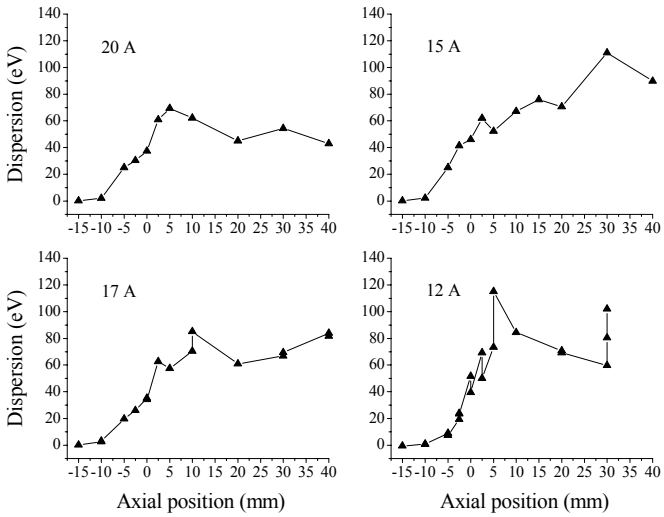


**Figure 8: Development of the spread in $Xe^+$ ion kinetic energy along the channel axis of the PPS®X000 thruster for various values of $I_b$ (change of the magnetic field).**

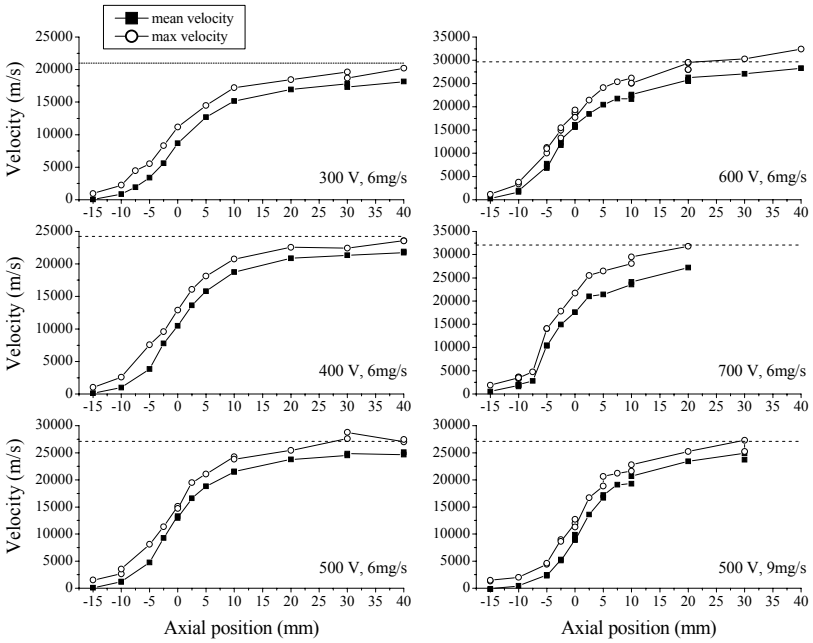


**Figure 9: $Xe^+$ ion axial velocity component as a function of the position along the channel axis of the PPS®X000 thruster for various values of $U_d$ and $\Phi_a$. Both the mean velocity (square) and the maximum velocity (at 10%) are plotted.**

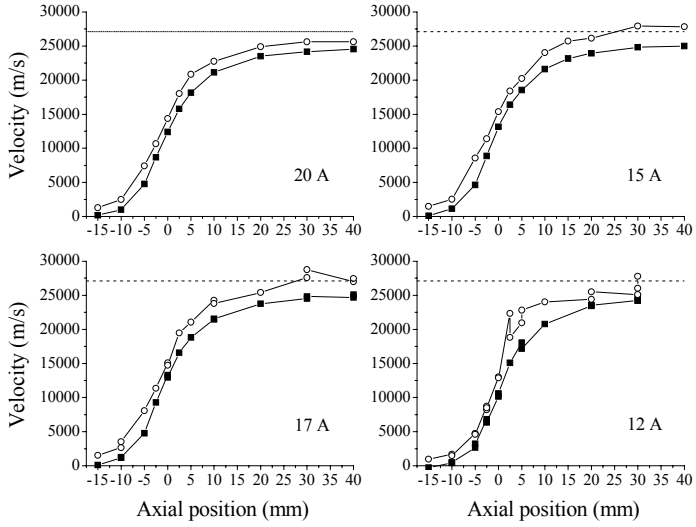


**Figure 10: $Xe^+$ ion axial velocity component as a function of the position along the channel axis of the PPS®X000 thruster for various values of $I_b$. Both the mean velocity (square) and the maximum velocity (at 10%) are plotted.**

**Overlap between the ionization and the acceleration layer**

The broadening of the $Xe^+$ ion VDF along the channel axis in the direction of the flow is a general feature for Hall effect thrusters that does depend neither on the size of the thruster nor on the input power.

Numerical simulations carried out with both a hybrid model and a kinetic (PIC) model show that the ion VDF broadening phenomenon finds its origin in the existence of a partial overlap between the ionization layer and the acceleration layer. Oscillations of the acceleration potential can amplify the phenomenon when they lead to an increase in the length of the overlap region. Computational simulations also indicate that the maximum of the velocity dispersion is reached at the end of the ionization layer.

The velocity dispersion is strongly influenced by the applied voltage. Both the dispersion and the degree of overlap increase with the voltage.

Our works reveal that in a Hall effect thruster, ionization and acceleration processes are well mixed up and they influence each other. It is therefore difficult, if not impossible, with a classical HET design and architecture to control in an independent manner the thrust (ionization) and the specific impulse (acceleration).

### B. Mean velocity and maximum velocity

The evolution of the $Xe^+$ ion mean and maximum (at 10%) velocity as a function of the axial position x is displayed in Fig. 9 and 10 for several values of $U_d$, $I_b$ and $\Phi_a$. In Fig. 9 and 10 the dashed line correspond to the ion velocity obtained assuming a full conversion of the potential $U_d$ into kinetic energy. This velocity is often referred to as the maximum achievable velocity.

The mean velocity is close to the theoretical limit but always below to fulfill the energy conservation principle. The length of the acceleration layer is around 40 mm. Note that the measurement at 700 V is not all-accomplished yet; the final ion velocity may be higher than the one visible in Fig. 9. The shape of the velocity profile depends on the applied voltage: the gradient is steeper when $U_d$ is ramped up and the whole profile is shifted towards the anode.

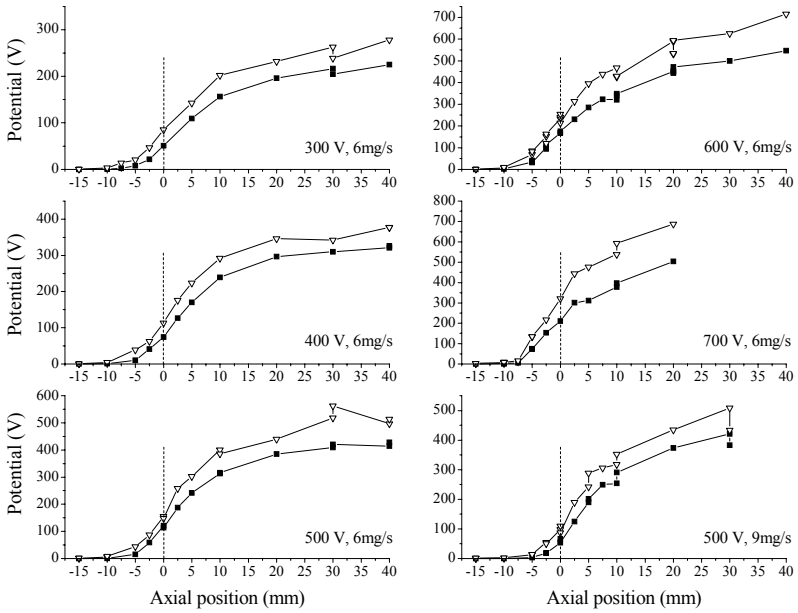


**Figure 11: Distribution of the acceleration potential along the channel axis of the PPS®X000 thruster for various values of $U_d$ and $\Phi_a$. The potential curve is derived from the mean velocity (square) and the maximum velocity (triangle).**

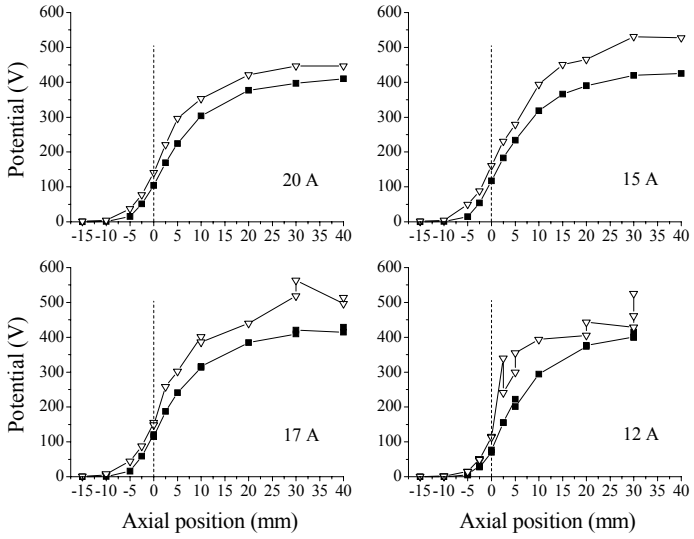


**Figure 12: Distribution of the acceleration potential along the channel axis of the PPS®X000 thruster for various values of $I_b$. The potential curve is derived from the mean velocity (square) and the maximum velocity (triangle).**

The magnetic field has a little influence on the velocity, however, the velocity profile slightly moves upstream when B increases. The gas flow rate has almost no effect on the velocity. The same tendencies were observed with the PSS100 thruster.

The maximum ion velocity $v_{max}$ is often above the theoretical limit given by $U_d$, especially at high voltage. Therefore there is a non negligible fraction of $Xe^+$ ions that have a kinetic energy larger than the applied potential energy. Such ions are also found with a PPS100 thruster. The fraction of very fast ions seems to increase with $U_d$. The origin of fast ions is not yet clear. Charge-exchange process between atom and/or $Xe^+$ ions and multiply-charged ions like $Xe^{2+}$ and $Xe^{3+}$ is a possible explanation. $Xe^+$ ions could also acquire a very large speed due to oscillations of the electric field as suggested by numerical simulations. Note that as a counterpart of fast ions, very slow ions are always observed in the discharge of a HET, see e.g. Ref. 3 and 4. Oscillations of the electric field can explain both the existence of very slow and very fasts ions.

### C. Acceleration potential and electric field

The acceleration potential $U_{acc}$ is calculated according to the formula:

$$\frac{1}{2} m v^2 = e U_{acc} . \tag{5}$$

Acceleration potential profiles along the channel axis are displayed in Fig. 11 for various voltages and propellant mass flow rates. Most of the acceleration occurs outside the channel whatever the operating parameters. The potential gradient becomes steeper when $U_d$ rises. The potential moves upstream with $U_d$ and downstream with $\Phi_a$, as can be seen in Fig. 11. In other words, the part of the acceleration potential located inside the channel increases with $U_d$ and decreases with $\Phi_a$. In all cases, a large fraction of the potential $\sim 70 - 80$ % is located outside the channel. A similar remark holds for the PPS100 thruster.

In Fig. 12, acceleration potential profiles along the channel axis are shown for various coil currents, which means for various magnetic field strengths. The magnetic field has a little impact on the potential, however, the fraction of the potential located inside the channel increases a bit with $I_b$. This effect is much more pronounced with the PPS100 Hall thruster.

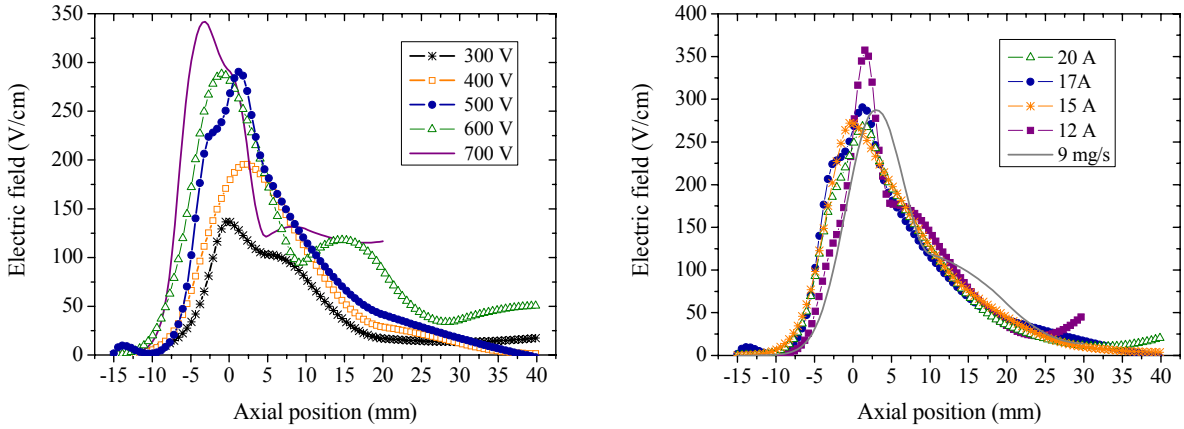


**Figure 13: Acceleration electric field as a function of the applied voltage (left) and of the coil current and gas flow rate (right) for the PP®SX000 thruster. The electric field is calculated from the mean velocity of the $Xe^+$ ion VDF.**

The electric field in axial direction $E_x$ is the derivative of acceleration potential:

$$E_x(x) = \frac{dU_{acc}(x)}{dx} = \frac{m}{e} v(x) \frac{dv(x)}{dx}. \quad (6)$$

In order to numerically compute $E_x$, it is necessary to smooth the potential curve and to interpolate the resulting curve using e.g. cubic splines. The shape of $E_x$ is sensitive to the data treatment procedure. The electric field distribution along the channel axis is shown in Fig. 13 for all studied operating conditions.

The magnitude of $E_x$ increases with $U_d$. The maximum of $E_x$ is shifted upstream when $U_d$ is ramped up. A large part of the electric field is outside the channel. Changing the magnetic field does not affect much the electric field but when the B field is weak. When the gas flow rate mounts the electric field distribution moves downstream but its shape is not modified.

**$Xe^+$ ion acceleration**

The length of the acceleration region is around 30 – 40 mm for the PPS®X000 and the PPS100 thrusters. A large fraction of the acceleration potential ~ 70 – 80 % is located outside the channel. This property seems very general for thrusters with the usual SPT architecture. It does not depend upon the thruster dimensions. It depends a little upon the operating conditions as the potential – the electric field – is shifted upstream when the applied voltage increases.

Most of the acceleration electric field is localized within a narrow area in the vicinity of the channel exhaust. This work also reveals that a part of the ionization process occurs in a region of strong electric field, especially at high voltage, which is a weak point for HET in terms of performance level.

Non negligible fractions of very slow ($Ec << e\,U_d$) and very fast ($Ec >> e\,U_d$) $Xe^+$ ions are always observed in the two studied Hall effect thrusters. Physical mechanisms at the origin of their production are still unknown. However, as suggested by hybrid and PIC numerical simulation outcomes, oscillations of the electric field could be an explanation.

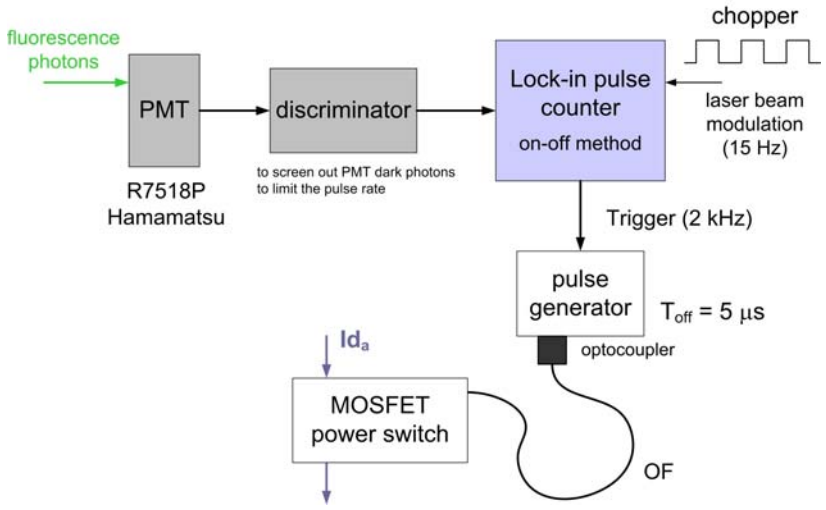


**Figure 14: Block diagram of the lock-in pulse counting system used in this work to measure the time-resolved $Xe^+$ ion VDF by means of LIF spectroscopy. The PMT is placed behind a 20 cm focal length monochromator.**

## V. Temporal characteristics of the $Xe^+$ ion VDF

### A. Interest in studying the time evolution of the VDF

It is well-established that the E×B discharge of a Hall effect thruster is strongly non-stationary. The discharge current oscillates over a broad frequency range that stretches from 10-20 kHz ("breathing" oscillations) up to 100 MHz (oscillations due to electron motion), each characteristic oscillation being linked to a specific physical process. The highly non-stationary nature of the plasma is a direct consequence of a complex physics at work at all levels in such a magnetized discharge. It appears in particular of great interest to investigate the temporal behavior of the $Xe^+$ ion VDF over time spans below or in the order of the time period of low-frequency plasma oscillations (50 – 100 µs) as the latters are the most intense ones. The time-averaged VDF certainly hides a rich and intricate ion dynamics that must be brought to light and compared to numerical outcomes of HET models in order to gain knowledge about the physics of such a complex plasma medium.

To achieve the measurement of the time-resolved $Xe^+$ ion VDF in a HET, it is necessary to develop a LIF spectroscopy bench able to produce and detect photons with a time resolution around 1 µs. In normal operating conditions of a HET, the number of fluorescence photons generated at 541.9 nm with a continuous laser beam of a few mW of power tuned at 834.7 nm is in the order of $10^{-3}$ per µs. Under identical conditions, the number of background photons generated by the plasma at 541.9 nm during 1 µs is typically 10. That means a ratio of $10^4$ between the two signal amplitude. The laser system must therefore be able (i) to detect a tiny amount of photons hidden in a strong background (ii) to determine with a high accuracy the exact moment in time fluorescence photons have been produced.

### B. Lock-in photon counting system

The pulse (or photon) counting technique allows to detect very low level signal with an excellent time resolution. When combined to a modulation of the laser light intensity (on-off cycle), the pulse counting technique can distinguish between LIF photons and spontaneous emission photons. The technique is known as the time-resolved pulse counting lock-in detection technique[7].

The laser bench is the same as the one used to measure the time-averaged VDF. The light collection branch stays also unchanged. The fluorescence radiation is carried away by means of a 200 µm core diameter optical fiber towards a 20 cm focal length monochromator. The lock-in amplifier is now replaced by a pulse-counting system developed by N. Sadeghi together with B. Pellisier. Details about the technique can be found in Ref. 7. We here briefly outline the main characteristics and settings of the system.

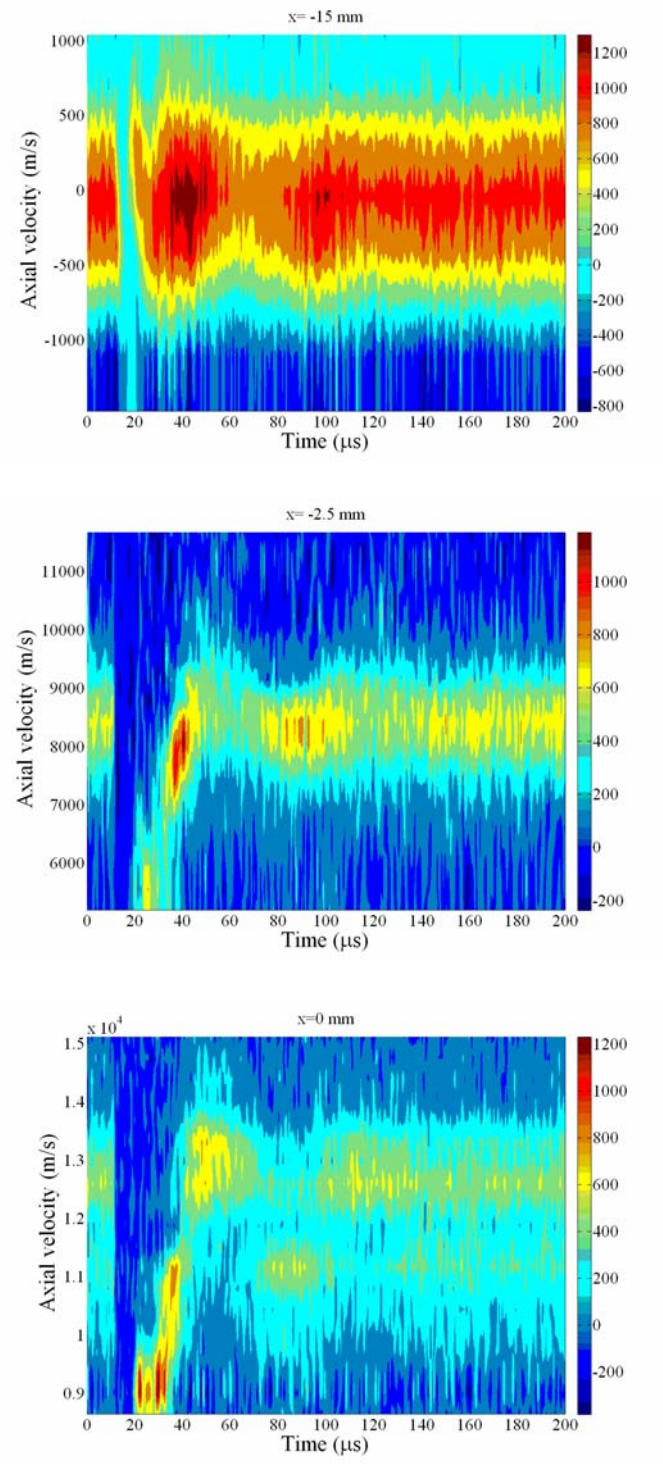


**Figure 15: Contour map of the $Xe^+$ ion axial VDF as a function of time for three different positions along the channel axis of the PPS®X000 Hall thruster: x = -15 mm, x = -2.5 mm and x = 0 mm. The operating conditions are :$U_d$ = 500 V, $I_b$ = 17 A and $\Phi_a$ =6 mg/s.**

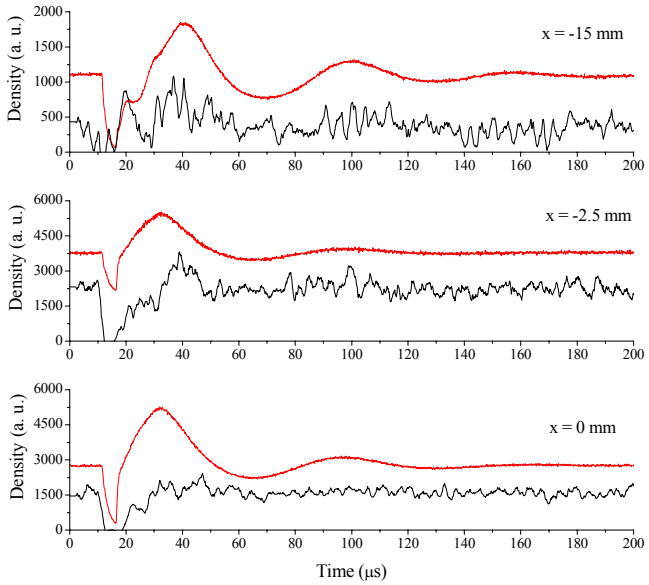


**Figure 16: Evolution in time of the metastable $Xe^+$ ion relative density for three positions along the channel axis of the PPS®X000 Hall thruster. The density is given by the VDF area. Also shown is the emission profile at 541.9 nm.**

A block diagram of the pulse counting system is shown in Fig. 13. Photons are detected by means of a high gain low noise PMT (R7518-P from Hamamatsu). A fast amplifier and discriminator module (9302 from Ortec – 100 MHz counting rate) is used to screen out PMT dark photons, to limit the pulse rate thus avoiding saturation of the counting system and to transform any single event (photon) into either a NIM or a TTL pulse. Pulses are subsequently treated by the lock-in pulse counter device, which counts events as a function of time. A trigger starts the counter which segments photon count data into sequential time bins (up to 32 kbins are available). The width of the bins can be set from 10 ns to 655 μs. The instrument records the number of photons that arrive in each bin. In order to greatly improve the S/N ratio, the counter is able operate in real-time counting-decounting mode. The laser beam intensity is modulated at low frequency (15-20 Hz) by means of a mechanical chopper. Each pulse recorded when the laser is propagating through the plasma is added to the time series (laser on: signal = LIF photons + background photons). Each pulse recorded when the laser is stopped is subtracted to the time series (laser off: signal = background photons only).

A 2 kHz trigger signal generated by the counter itself was used to define the start of the measurement cycle. The time resolution (width of each bin) was set to 100 ns and 5000 bins were used. The duration of one measurement cycle is therefore 500 μs that correspond to about 6 times the period of LF current oscillations of the PPS®X000 thruster operating at 500 V, 17 A and 6 mg/s (f = 13.7 kHz). In order to obtain a reasonable S/N ratio, light was accumulated over 1 million cycles.

For this first set of experiments, we decided to investigate the ion flow dynamics before and after a fast shut off of the anode current. It was therefore possible to examine the temporal characteristics of the ion VDF during plasma breakdown and ignition as well as during forced and free current oscillations.

The anode current is shut off during 5 μs at 2 kHz by way of an optically driven fast power switch based on a MOSFET[8]. The power switch is operated by remote control by the counter. There is no synchronization between the power shut down cycle and the discharge current waveform. In other words, the anode current is switched off randomly in time.

The procedure to obtain the time-resolved VDF is the following:

- the laser is fixed at a given wavelength λ that correspond to a certain ion velocity group δv. The extent (dispersion) of the velocity group results from the spectral width of the laser beam and from the thermal

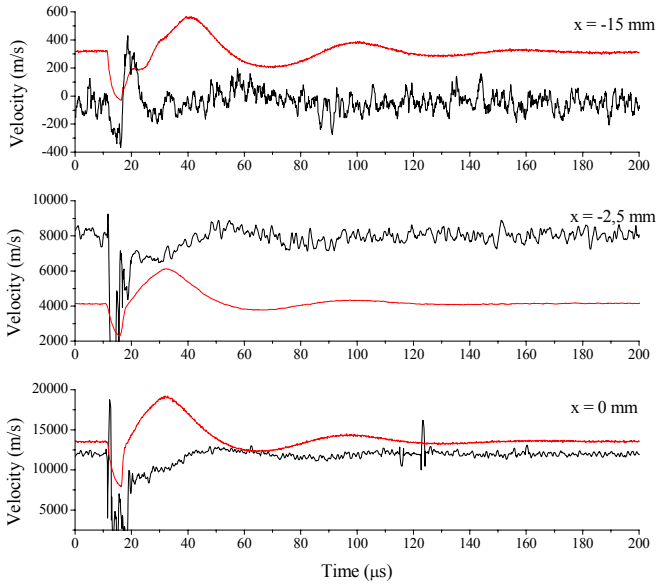


**Figure 17: Evolution in time of the metastable $Xe^+$ ion mean velocity for three positions along the channel axis of the PPS®X000 Hall thruster. Also shown is the profile of the light emission at 541.9 nm.**

expansion of the laser cavity. A feedback loop allows to minimize the shift of the laser wavelength. The dispersion is thus around 10 m/s.

- the pulse counter is used to record the number of fluorescence photons induced by excitation of metastable ions at λ. That means we follow the evolution in time of the velocity group δv.
- after one million cycles the laser wavelength is changed and a new measurement starts.

To obtain a smooth ion VDF about 15 to 20 different wavelengths are used.

### C. Contour map of VDF(t)

In Fig. 15, contour plots of the time evolution of the $Xe^+$ ions are displayed for three different positions along the channel axis, respectively x = -15 mm (ionization zone), x = -2,5 mm (beginning of the acceleration zone) and x = 0 mm (channel exit). The operating parameters of the PPS®X000 5 kW-class Hall thruster are kept fixed: $U_d$ = 500 V, $I_b$ = 17 A and $\Phi_a$ =6 mg/s.

The anode current is always switched off at t = 11.3 µs; the thruster starts again at t = 16.3 µs. The first oscillation is forced. The ion production is large at plasma ignition as the channel is entirely filled up with xenon atoms. Slow ions, in fact ions at rest, are always produced at ignition. As can be seen in Fig. 15, the $Xe^+$ ion VDF in axial direction changes in time. That means the acceleration potential, and the electric field, are also varying at the time scale of low-frequency current oscillations. Note that when outside the acceleration layer (x = -15 mm), only the amplitude of the VDF is changing.

### C. Evolution in time of the density, mean velocity and dispersion

The evolution in time of various averaged quantities is plotted in Fig. 16, 17 and 18 for the three aforementioned positions along the channel axis. The relative metastable ion density is given by the area of the VDF. The mean velocity and the velocity dispersion (p parameter) are computed from respectively the first and the second order moment of the velocity distribution.

As can be seen in Fig. 16, the ion density is oscillating in time meaning that the ionization rate is varying in time. As already mentioned, the ion density is the highest right after plasma ignition.

The time evolution of the mean velocity is shown in Fig. 17. At x = -15 mm, the velocity oscillates around 0 as this point is outside the acceleration layer. At x = -2.5 mm and x = 0 mm, the mean velocity oscillates. The velocity

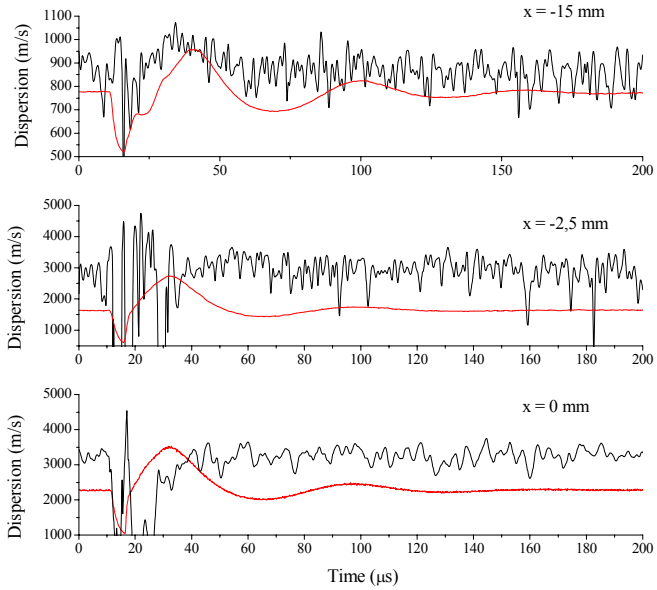


**Figure 17: Evolution in time of the metastable $Xe^+$ ion axial velocity dispersion (p parameter) for three positions along the channel axis of the PPS®X000 Hall thruster. Also shown is the profile of the light emission at 541.9 nm.**

is delayed with respect to the emission signal. The velocity change is however small, in the order of a few percents. The oscillation of the mean ion velocity may results from either a back and forth motion of the ionization and acceleration layers or a change in the electric field amplitude.

As can be seen in Fig. 18, the velocity dispersion does not vary much in time but at current shut off and restart. At the channel exhaust, the energy spread is almost constant with a value around 40 eV.

The analysis of the temporal characteristics of time-averaged quantities is too rough to reveal accurate details about the $Xe^+$ ion dynamics in a HET. It is therefore necessary to examine with care the behavior of each velocity group and to correlate observations realized at different locations. Moreover, the measured evolution in time of the ion VDF must be compared with outcomes of hybrid and kinetic models.

## VI. Conclusion

The LIF spectroscopy studies on the time-averaged $Xe^+$ ion VDF performed with the PPS100 and the PPS®X000 Hall effect thrusters show the impact of the applied voltage, the magnetic field, the xenon mass flow rate and the thruster dimensions on kinetic energy spread and acceleration potential profile. A change in ion flow properties is observed at high voltage ($U_d \geq 600$). These works give information about the coupling between the ionization and the acceleration layers. Moreover, they also reveal the existence of very slow and very fast ions.

For the first time ever, the temporal characteristics of the $Xe^+$ ion VDF was observed in the E×B discharge of a HET in the course of low-frequency current oscillations. Measurements were achieved with a 100 ns time resolution by means of a lock-in pulse counting LIF spectroscopy technique. A first examination of the evolution in time of the ion VDF indicates that the acceleration potential distribution, and the electric field, oscillates in time and/or in space. Data analysis just started and numerous efforts are still needed to better understand the ion dynamics. The behavior of each probed velocity group must be scrutinized in order to understand in which way the potential is changing. Experimental data must also be compared to numerical simulations. Finally, it will certainly be necessary to carry out new experiments in the near future.

## Acknowledgments

Works are performed in the frame of the joint research program GdR CNRS/CNES/SNECMA/Universities 2759 “Propulsion Spatiale à Plasma”.

## References

[1] W.A. Hargus, Jr. and M.A. Cappelli, *Appl. Phys. B*, Vol. 72, 2001, pp. 961-969.
[2] N. Dorval, J. Bonnet, J.P. Marque, E. Rosencher, S. Chable, F. Rogier, and P. Lasgorceix, *J. Appl. Phys*, Vol. 91, 2002, pp. 4811-4817.
[3] D. Gawron, S. Mazouffre, L. Albarède, N. Sadeghi, Proceedings of the 42nd AIAA/ASME/SAE/ASEE Joint Propulsion Conference & Exhibit, 9 - 12 July, 2006, Sacramento, California, *AIAA paper 06-4473*.
[4] D. Gawron, S. Mazouffre, N. Sadeghi, A. Héron, submitted to *Plasma Sources Sci. Technol.*, 2007.
[5] S. Mazouffre, A. Lazurenko, P. Lasgorceix, M. Dudeck, S. d’Escrivan, O. Duchemin, Proceedings of the 7th International Symposium on Launcher Technologies, Barcelona, Spain, April 2-5, 2007, *paper O-25*.
[6] J. Kurzyna, S. Mazouffre, A. Lazurenko, L. Albarède, G. Bonhomme, K. Makowski, M. Dudeck, Z. Peradzyński, *Phys. Plasmas*, Vol. 12, 2005, 123506.
[7] B. Pellissier, and N. Sadeghi, Rev. Sci. Instrum., Vol. 67, 1996, pp. 3405-3410.
[8] V. Vial, S. Mazouffre, M. Prioul, D. Pagnon, A. Bouchoule, *IEEE Transactions on Plasma Science*, Vol. 33, 2005, pp. 524-525